Research Article *http://dx.doi.org/10.4314/mejs.v10i1.3*

Polypropylene Nano-composites at High Strain Rate Impacts: Characterization, Failure Modes, and Modeling

Shishay Amare Gebremeskel[1*], Neelanchali Asija[2], Hemant Chouhan[3] and Naresh Bhatnagar[2]

[1]School of Mechanical and Industrial Engineering, Ethiopian Institute of Technology-Mekelle, Mekelle University, Mekelle 231, Ethiopia (*shishay.amare@mu.edu.et).

[2]Department of Mechanical Engineering, Indian Institute of Technology Delhi, Hauz Khas, New Delhi 110016, India.

[3]Department of Mechanical Engineering, Amity University, Uttar Pradesh, 201313, India.

ABSTRACT

As a major challenge, development of light-weight fibre reinforced polymer (FRP) composite body armour, characterization of candidate matrix polymers at high strain rate impact is the focus in this research. Polypropylene (PP) and the nano-composites with 1-5% by weight of NC (nanoclay) platelets are the candidates considered. In the characterization phase, high strain rate impact and quasi-static loading tests were performed to figure out the limiting (failure) responses. Comparison between the material systems is, subsequently, made to nominate one matrix configuration. Enhancements of mechanical properties with increase in weight percentage of the nanoparticles are observed at both quasi-static and dynamic loadings. Observations of dispersed imposed failure modes, development of novel model for failure modulus and evaluation of peak strength values are also attempted.

Keywords: Nano-composite, Impact behaviour, Analytical modelling, Polypropylene, Failure mode.

1. INTRODUCTION

The research endeavours to develop a light-weight armour material system at IIT Delhi brought a focus on FRP (fiber reinforced polymer) composites. The design and development work of an armour material system requires appropriate selection of performance properties of different matrix materials. However, the strain rate dependence of matrix part of FRP composites makes the job tougher as characterizations are required at every level of strain rate for various applications. Experimenting candidate thermoplastic polymers and their composites at high strain rate impacts are required prior to designing the material system.

Like any other material systems, thermoplastic based composites require structural, physical, mechanical and other characterizations. The quasi-static punch shear test revealed at University of Delaware on four different polymers, namely nylon 6/6, polycarbonate (PC), ultra high molecular weight polyethylene (UHMWPE) and PP show that PP has the highest specific energy (energy per

Submitted on: 25-12-2017 ***Accepted on: 23-03-2018***

unit mass) dissipation next to nylon 6/6, which indicates that PP could be one of the promising polymers where energy dissipation is important as nylon is usually hygroscopic. Depending on the type of process and experiment used, particular type of PP and nature of the clay particles, improvements reported in different studies are not identical. However, they indicate a generally converging trend. For example, (Shariatpanahi et al., 2009) revealed improvements of 15% and 22% in modulus at quasi-static and impact loadings, respectively.

The necessity of separate characterization of polymers and polymer based composites at high strain rate loadings was also recommended as extrapolation of low strain rate property data for high strain rate designs of polymer based structures may not be acceptable (Kukureka and Hutchings, 1981). The reason put in place is that polymers usually undergo non uniform elastic-plastic way of deformations. Therefore, study of behaviors of polymers under ballistic or high strain rate impacts, regardless of their quasi-static properties, is vital to decide the right polymer/s for matrix purpose of an armor system. Generally speaking, the ability of polymers to absorb and mitigate impact energy (Qiao, Yang and Bobaru, 2008) and the new, clay-induced, mechanism of plastic deformation (Yuan and Misra, 2006) boost toughness of the nano-composites. As per the report, the 'crazing and vein-type' failure mode of neat PP was changed to 'micro void coalescence-fibrillation' mode due to the dispersed phase.

Input information for this research is limited as the military nature of impact studies with ranges of strain rates of high and beyond might be a reason for it to be classified. Even no constitutive model which could be, optionally, used to predict high strain rate impact responses of thermoplastic polymers and composites exist. However, understanding was taken from existing quasi-static loading models for elastic modulus: general rule of mixture, Halpin-Tsai model (Jones, 1999), Ji model (Ji et al., 2002), and Takayanagi model (Okamoto and Takayanagi, 1968). A three-phase mathematical model developed by Ji observed to be in good agreement with experimental results by (Cauvin et al., 2010) become thought-provoking in developing new model in this study. Nonetheless, the interface state which was considered as a third phase, in Ji's model, may be difficult to physically quantify in thickness as it is not consistent with the very definition of phase in matter, if not taken in other sense.

Evaluation of peak strength values of neat PP and PP nano-composites was also performed by adopting existing models. Although some modeling studies exist (Johnson and Cook, 1985; Silva, Cismasiu and Chiorean, 2003, 2005; Zhu and Narh, 2004; Odegard, Clancy and Gates, 2005; Park,

Yoo and Chung, 2005; Valavala and Odegard, 2005; Grujicic et al., 2007; Yong, Iannucci and Falzon, 2010; Omar, Akil and Ahmad, 2011), two of them (Johnson-Cook (Johnson and Cook, 1985) and Omar et al. (Omar, Akil and Ahmad, 2011)) are found with less experimental variables and easier to adopt. Johnson-Cook model was primarily developed to study strain rate dependence of isotropic metals (Johnson and Cook, 1985; Rajendran, 1994; Vedantam et al., 2006) at strain rates to the order of 10^3 s^{-1} and above. However, Omar et al. model is applied to study strain rate sensitivity of neat thermoplastic polymers. To meet the central objective of this study, the material systems are mainly compared for the performances at high strain rate impacts.

2. METHODOLOGY

The materials considered, the processes followed to prepare test specimens, the experimental techniques, and the data analysis methods are presented in this section.

2.1. Materials and Processing

Particular PP 'REPOL C015EG' supplied from 'Reliance Industries Limited, India' is used as basic material system of the study. As per ASTM D-1238, the MFI (Melt Flow Index) of this typical thermoplastic polymer is 1.5g/10min at 230^{o}C. The NC (nanoclay) powder used as filler is an MMT (montmorillonite) designated as Cloisite® 15A. It was supplied from 'Southern Clay Products Inc., USA'.

Granules of neat PP were melt-mixed with particular amount of NC fillers, using twin screw extruder machine, from which granules of the nano-composites were produced. Then tensile test specimens of all material systems were prepared using an injection moulding machine. Sheets of all material batches were also produced using an extruder machine. Out of the extruded sheet rolls, specimens for SHPB (split Hopkinson pressure bar) experiments were cut. Graphic presentation of materials and the processes can be found in a previous publication (Gebremeskel and Bhatnagar, 2015). Prior to the main mechanical tests distribution of particles within the matrix was checked through bulk morphologies of specimens, reported in previous paper (Gebremeskel et al., 2017), shown to be similar to the images reported by (Hedayati and Arefazar, 2009).

Neat PP and PP-nanocomposites (with NC weight fractions varying from 1-5%) are experimentally investigated. The nanoclay platelets are limited to 5wt% to prevent agglomerations that may happen while melt-mixing of higher percentages. Only three material systems, namely, neat PP, PP+2wt%NC (PP reinforced with 2% by weight of nanoclay), and PP+5wt%NC (PP

reinforced with 5% by weight of nanoclay), are considered in the detailed discussion of responses. However, results of all experimented material systems including PP+1wt%NC (PP reinforced with 1% by weight of nanoclay), PP+3wt%NC (PP reinforced with 3% by weight of nanoclay), and PP+4wt%NC (PP reinforced with 4% by weight of nanoclay), are included in modelling.

2.2. Mechanical Testing and Data Scrutiny

All experiments were, deliberately, carried out at room temperatures of 21±3^{o}C since no temperature effects were considered. Quasi-static load experiments were performed using Zwick/Roell UTM machine as per ASTM D 638 at a particular strain rate of 10^{-2} s^{-1}. While, a SHPB developed in-house was employed for the high strain rate impact experimentation following the classical calibration rules. Specifications of this particular SHPB setup are presented in previous article (Gebremeskel et al., 2014). Strain rates of upper bound of high (order of 10^{3} s^{-1}) and lower bound of very-high (10^{4} s^{-1}) were achieved. Pressure-velocity calibration for medium-length striker bar was considered to set the required impact pressure and compute corresponding impact velocity. Three mechanical properties, peak stress, modulus (identified as 'elastic modulus' for quasi-static tests and 'failure modulus' for impact tests) and toughness are, mainly, deliberated for comparison purposes and to observe effects of loading types and the dispersed particles. Data scrutinizing procedures and formulae to obtain the stated properties from both quasi-static and impact loadings are presented in previous article (Gebremeskel and Bhatnagar, 2015).

3. RESULTS AND DISCUSSION

Mechanical responses of neat PP and PP nano-composites at both quasi-static and impact loadings are presented. Respective deformation and failure modes and effects of dispersed particles in this regard are also discussed. Finally, average response values of strain rates, moduli, and peak strengths are extended to model PP nano-composites at impact.

3.1. Characterization and Failure Modes at Quasi-static Loading Rate

The elasto-plastic nature of deformation of all material systems are observed beyond 20 MPa (Fig 1) reaching the peak stress (yield strength in case of polymer based materials) shortly.

Observing the deformation process and failure conditions, neat PP (Fig 1a) shows a kind of crazing transferred to short bands of fibrils or ligaments, PP+2wt%NC (Fig 1b) experienced an in-plane shearing behavior and layer-by-layer yielding prompted by the interfacial separation between the

platelets and the polymer (matrix), and PP+5wt%NC (Fig 1c) resembled the modes shown in cases of both neat PP and PP+2wt%NC leading to extended strain to failure.

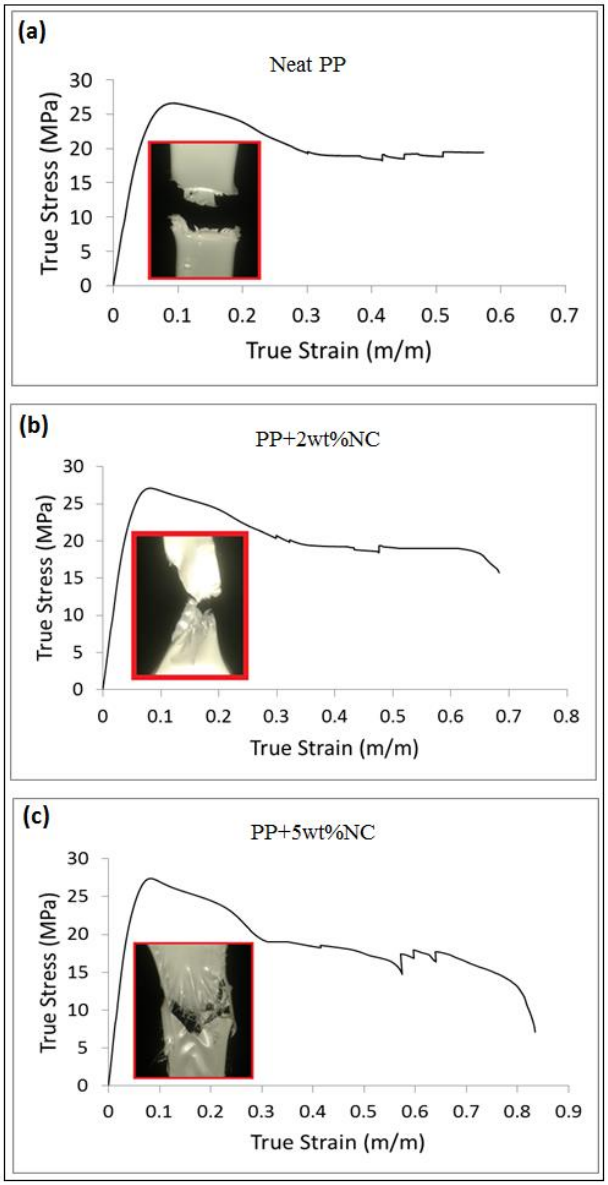

Figure 1. Stress-strain graphs and failure modes at quasi-static rate of loading.

3.2. Characterization and Failure Modes at High Strain Rate Impacts

High strain rate impact experiments were performed by identifying the maximum firing gas pressure and limiting impact velocity of a particular striker bar beyond which fracture of the test specimen happens. Thus, thickness effects and the limiting (failure) properties are discussed in the next sections for the selected material systems (neat PP, PP+2wt%NC and PP+5wt%NC).

Table 1. Summary of dynamic responses of the studied material systems.

Material systems	***Specimen thickness levels***	***Firing pressure (bar)***	***Impact velocity (m/s)***	***Strain rate (s^{-1})***	***Peak stress (MPa)***	***Peak strain (m/m)***	***Failure modulus (GPa)***	***Toughness (MJ/m^3)***
Neat PP	Low	1.60	32.0	22673	283	0.044	6.38	198.10
	Medium	1.90	34.3	15260	255	0.072	3.54	171.30
	High	2.10	35.7	8206	167	0.110	1.52	101.20
	Averages of responses			15380	235	0.075	3.81	156.87
PP+2wt%NC	Low	1.7	32.8	19938	306	0.013	23.54	211.2
	Medium	1.9	34.3	13939	279	0.028	10.07	192.3
	High	2.2	36.4	7661	173	0.041	4.22	127.3
	Averages of responses			13846	253	0.027	12.61	176.9
PP+5wt%NC	Low	1.9	34.3	18848	336	0.0085	39.0	303.4
	Medium	2.2	36.4	12902	316	0.0110	28.7	280.5
	High	2.3	37.1	6849	294	0.0137	21.5	261.3
	Averages of responses			12866	315.3	0.013	29.7	281.7

Three thickness levels namely, low (350 μm), medium (700 μm) and high (1400 μm) were prepared for all material systems. This was purposely made to affect the strain rate and examine the effects on the dynamic responses of each material system. Summary of the analyzed main mechanical responses of corresponding material systems at varying thicknesses and associated strain rates are given in table 1. Tabulated results, response plots, deformation and failure mechanisms of the material systems are discussed in the following sections.

3.2.1. Neat PP

The inverse proportionality of strain rate with specimen thickness given in classical SHPB theory is clearly observed in figure 2a. On the other hand, an increase in peak stress and decrease in peak strain are observed with increasing strain rate, as shown in figure 2b.

Similar to the peak stress, an increase in strain rate led to a rise in failure modulus 'E_f' and the amount of strain-energy absorbed per unit volume or toughness 'u'. In this main part of the study, high strain rate impact, strength and strain terms are referred as peak and modulus term is referred as failure, hence peak stress (σ_p), peak strain (ε_p) and failure modulus (E_f). The entire mechanics

in such high impact loadings extremely undermines elasticity and yielding. Thus, the important phenomena to deal with are absorption and dissipation of energy and that is why limiting (failure) impact responses are considered. Details of the dynamic responses and their average values for neat PP are included in Table 1. The average dynamic response values were deliberated for just comparison purposes with the other material systems, namely PP+2wt%NC and PP+5wt%NC.

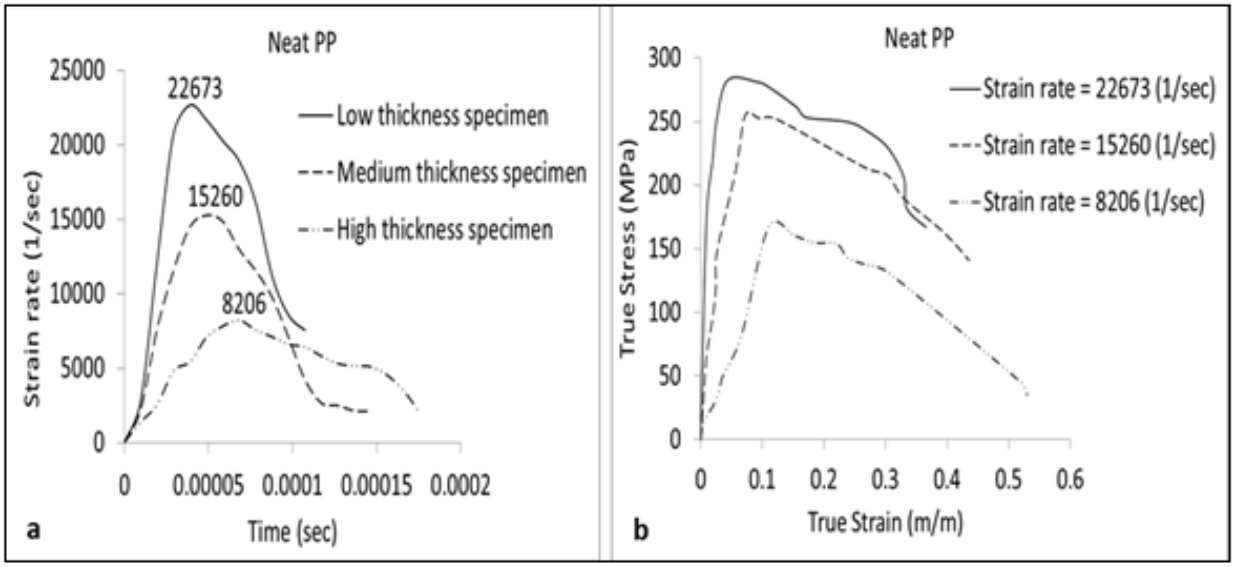

Figure 2. Impact responses of neat PP (a) strain rate at different thicknesses (b) stress-strain at different strain rates.

The impact stress-strain plots are shown to have successive wrinkles unlike to the case of smooth quasi-static loading curves. This is because of the very nature of the experiment, all about wave transport through the material and hence wave fluctuations are unavoidable (Li and Lambros, 2001). What is important to note is that the directional trend of data points to calculate failure modulus (E_f). Though the peak stress is found easier to pick, one third of the magnitude is recommended to be taken as yield stress for actual product designs. Generally, that is a much approximated value for polymer based material systems to start yielding at impact. In this work, the peak strength term is discussed instead of calculating for yield strength as energy absorption and dissipation are the major concerns in armor applications. This statement of clarity works for all dynamic stress-strain curves in all the material systems discussed herein.

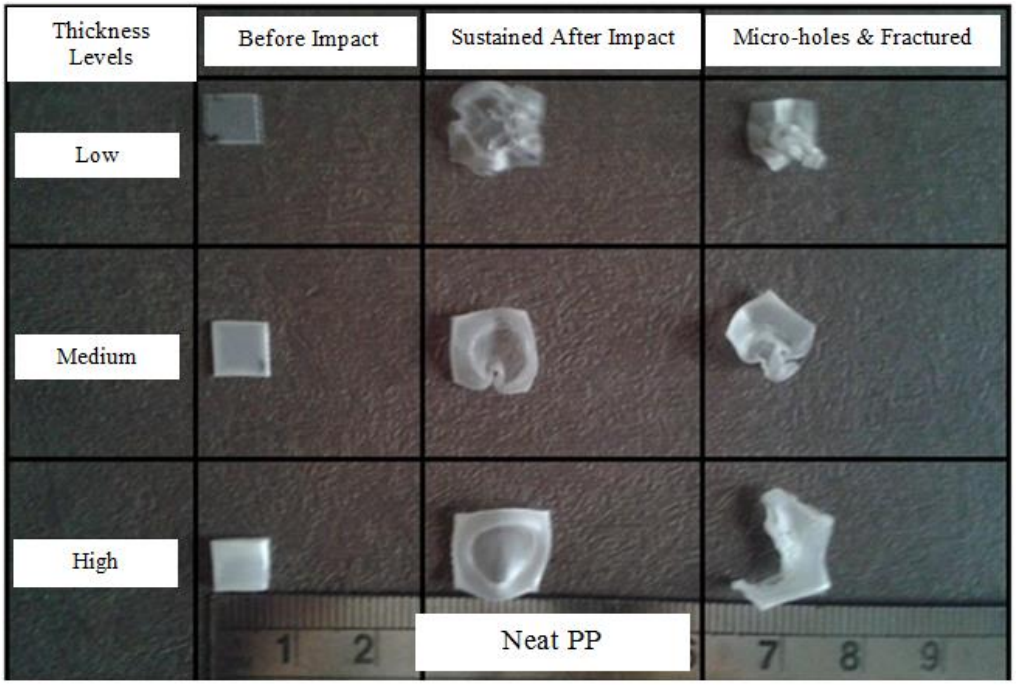

Figure 3. Deformation and fracture modes of neat PP at impact compression loading on SHPB.

A relatively wide range of plasticity of neat PP can also be swot from the deformation modes shown in Figure 3. Specimens in states of 'before impact', 'sustained after impact' and 'micro-holes & fractured' are depicted, corresponding to each thickness level: Thickness levels, which normally represent corresponding strain rates. The material system undergoes visco-plastic (plastic deformation associated with melting) deformation and fracture modes in the form of recoiling, multiple micro-holes and total rupture. The phrase 'sustained after impact' refers to a plastically deformed specimen with no holes and cracks. The deformation and damage can be correlated with the quantified responses. The increase in failure modulus, peak stress, toughness and reduction in peak strain with strain rate are attributed to decreased mobility of polymer chains (stiffened), molecular relaxation shift, change of rubbery-like regime to leathery-like one and rise in adiabatic heat, respectively (Omar et al., 2011). Moreover, the authors believed that the higher strain rate loadings, each completed at such ultra-short durations, do not allow the molecules to get displaced as significant as they do at lower strain rates. Hence, the material behaves like a rigid and brittle matter gaining higher stiffness and strength. Yet, the brittleness for that duration results in decreased peak strain.

3.2.2. PP+2wt%NC

The presence of dispersed nano-platelets throughout the polymer matrix has added effects on the inherent properties of the neat one on top of the effects posed by the nature of loading. Effect of 2% by weight of NC particles on PP, in particular, can be understood from the quantified values of the considered responses in this study. Though the trends of strain rate-time plots at varying specimen thicknesses, figure 4a, and stress-strain plots at varying strain rates, figure 4b, are similar to that of neat PP, PP+2wt%NC show relatively reduced strain rate and peak strain and improved failure modulus, peak stress and toughness.

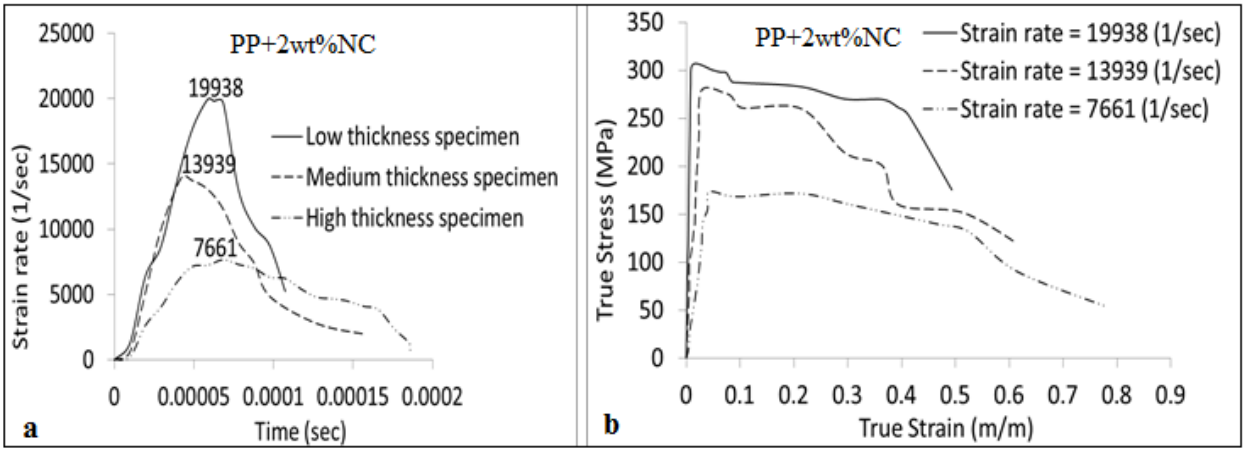

Figure 4. Impact responses of PP+2wt%NC (a) strain rate at different thicknesses (b) stress-strain at different strain rates.

Except for the medium thickness level which may be the result of the usually expected mixing flaws during compounding nano-particles with polymers, this material system required somehow higher limiting impact pressure and velocity. This condition and the relatively reduced strain rate and peak strain values than neat PP at every thickness levels are the result of the dispersed: contributing in hindering the mobility of material due to the Van Der Waals force and frictional effects developed on the platelet-matrix interfaces. The surface interactions posed, moreover, have got a stiffening effect revealed by the raised value of failure moduli and peak stresses. The presence of interface which makes surface detaching process obvious, when loaded enough, is another advantage of the nano particles for the material to experience relatively wider strain past the peak value and have significant effect on the strain energy absorption. Responses and corresponding average values are included in table 1.

The average values of responses given are extended for the comparison purpose of PP+2wt%NC with neat PP and PP+5wt%NC. Actual observation of deformations and damages of PP+2wt%NC at different strain rates (different thickness levels) are depicted in figure 5 to relate and discuss the mechanics.

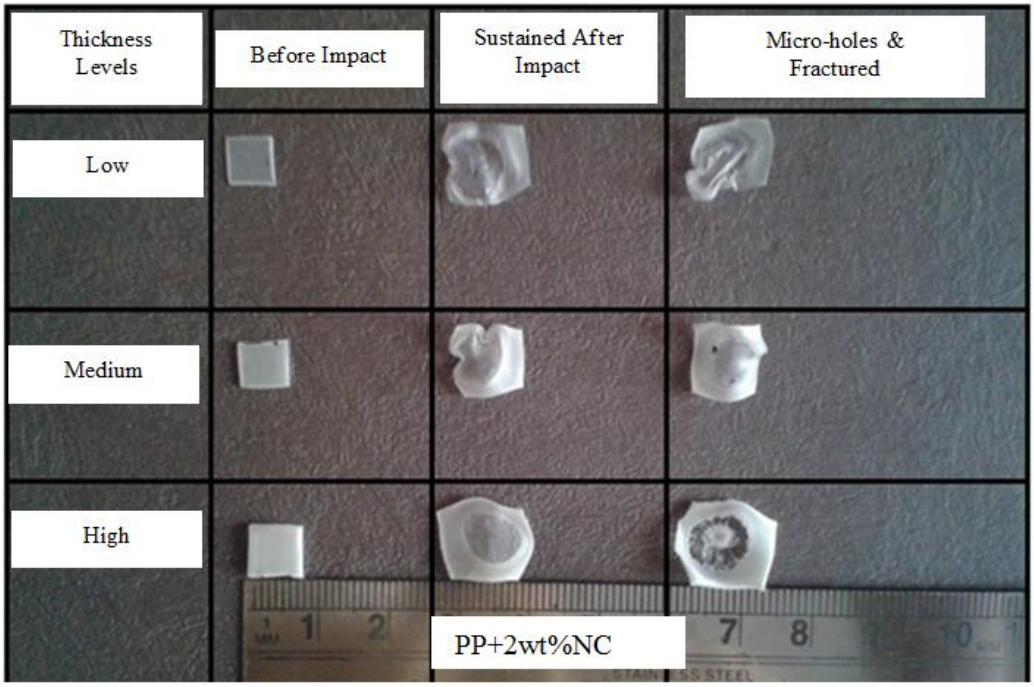

Figure 5. Deformation and fracture modes of PP+2wt%NC at impact compression loading on SHPB.

Somehow different modes of deformation and fracture compared to neat PP are observed in case of PP+2wt%NC. Looking at 'sustained after impact', primary visco-plastic deformation of the bulk material followed by platelet-matrix surface disintegration may be the main mechanics. When observed, the impacted area is clearer and transparent. This is because the particles are moved radially and accumulated around the periphery. However, fracture seemed to occur after secondary visco-plastic deformation following the weakened radial paths where the particles moved through. The stated nature of the mechanics can be well observed from the fractured 'high thickness' case having radial fibrils (ligaments), unlike in the case of neat PP.

3.2.3. PP+5wt%NC

Except for the highly increased effect-level induced by 5wt% nanoclay particles, this material system generally show similar mechanics of deformation and fracture to PP+2wt%NC. Specimen

thickness and strain rate also affect the responses in the same trend observed for both neat PP and PP+2wt%NC, as shown in figure 6 a &b. PP+5wt%NC requires the highest limiting impact pressure and velocity settings than the rest of the material systems. Due to the increased content of the nanoclay platelets, lowest average strain rate and peak strain values are recorded. However, the reinforcing and stiffening effect of 5wt% nanoclay put PP+5wt%NC to be top-notch of all considered material systems in peak stress, failure modulus and toughness.

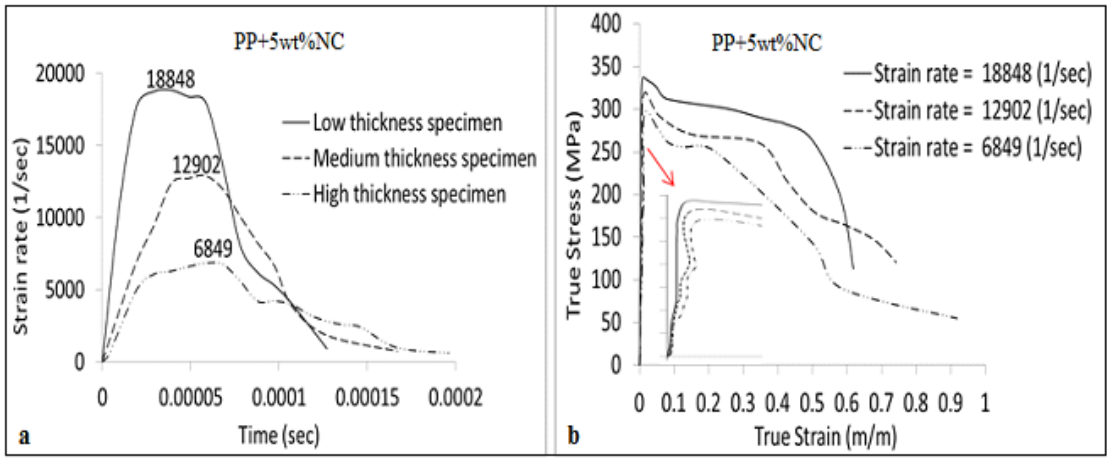

Figure 6. Impact responses of PP+5wt%NC (a) strain rate at different thicknesses, (b) stress-strain at different strain rates.

Average values indicated in table 1 are extended for comparison of the considered impact responses of PP+5wt%NC with neat PP and PP+2wt%NC. Thus, average-wise, PP+5wt%NC show improvements of 34% in peak stress, 680% in failure modulus, and 80% in toughness when compared to neat PP. Similarly, for the other material systems, deformations and damages of PP+5wt%NC at different strain rates (different thickness levels) are depicted in figure 7 for observation and discussion of the mechanics relating to the plots and quantified values.

Observing the "sustained after impact," PP+5wt%NC samples undergo a similar but more pronounced deformation mechanics to that of the PP+2wt%NC. The radial fibrillation mode of fracture, following secondary visco-plastic deformation, is evident here in this case also. Comparing the fractured 'high thickness level' of both PP+2wt%NC and PP+5wt%NC, more material is observed at the impacted area of the later which is attributed to the better reinforcing and strengthening effect of the 5% by weight content of NC platelets. Moreover, the recoiling after extreme deformation or fracture was shown to be common, significant at low thickness levels, for all material systems.

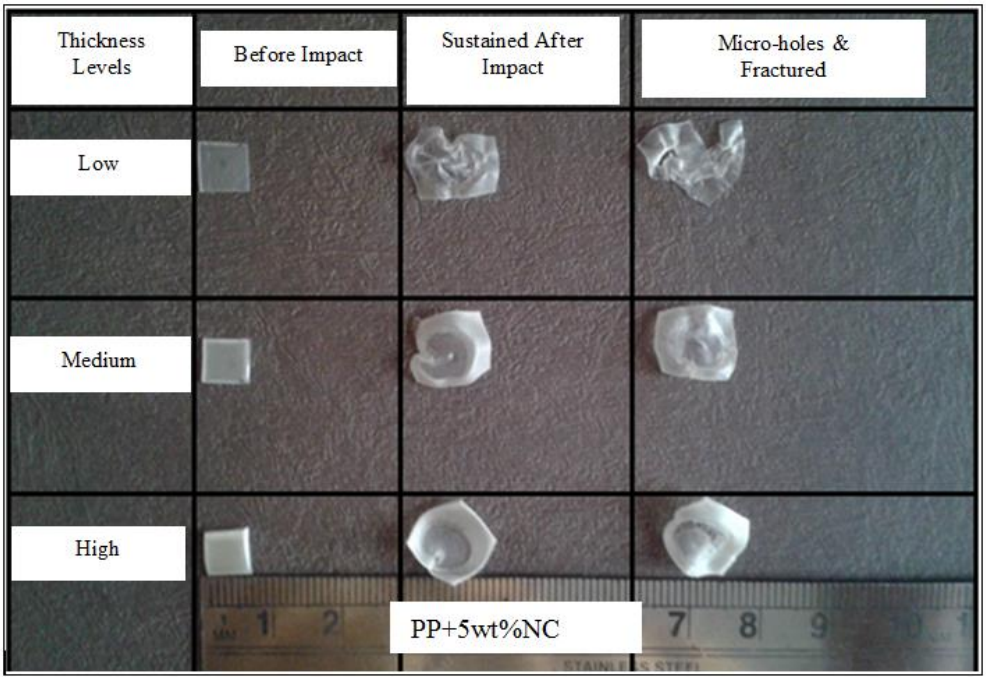

Figure 7. Deformation and fracture modes of PP+5wt%NC at impact compression loading on SHPB.

Table 2. Experimental results of all material systems considered in modeling.

Material systems	***Quasi-static Loading[a]***			***Impact Loading[b]***		
	$\dot{\varepsilon}_q\ (s^{-1})$	***E (GPa)***	σ_{qp} ***(MPa)***	$\dot{\varepsilon}_i\ (s^{-1})$	E_f ***(GPa)***	σ_{ip} ***(MPa)***
Neat PP	10^{-2}	0.83	26.70	$1.538*10^4$	3.81	235.0
PP+1wt%NC	10^{-2}	0.85	26.90	$1.430*10^4$	8.65	242.8
PP+2wt%NC	10^{-2}	0.89	27.10	$1.385*10^4$	12.61	253.0
PP+3wt%NC	10^{-2}	0.90	27.25	$1.320*10^4$	17.56	276.0
PP+4wt%NC	10^{-2}	0.91	27.31	$1.299*10^4$	24.00	296.5
PP+5wt%NC	10^{-2}	0.92	27.4	$1.287*10^4$	29.72	315.3

Note: [a]represented by subscript 'q'; [b]represented by subscript 'i' in nomenclatures.

3.3. Analytical Modeling

Development of new model of failure modulus and evaluation of peak strength using existing models is discussed here. Additional material systems, not considered on detailed discussions, were experimented in order to have enough number of experimental points and rationalize the models. Additional material systems are PP+1wt%NC, PP+3wt%NC and PP+4wt%NC. The models with errors <30% though are acceptable (Cauvin et al., 2010), further reduction demands continuous research.

Necessary average experimental results of all material systems used throughout the modeling process are presented in table 2. The tabulated experimental results show respective strain rate ($\dot{\varepsilon}$), modulus (E) and peak stress (σ_p) for both quasi-static and impact loadings.

3.3.1. Failure Modulus

The newly developed two-phase model of modulus is considered as an interface-induced stress-field. Surface theory is extended to support the existence of stress-field at the platelet-matrix interface instead of considering the interface as third phase which is difficult to quantify the thickness. The PP matrix was considered as adsorbate and the nanoclay platelets as adsorbent surfaces. Parametric size of PP crystals, generally known to be around 4.2 Å, is small enough to be considered as adsorbate compared to nanoclay platelet surface dimensions. An adsorbate attains closest behaviors at the nearest vicinity to the surface of an adsorbent, provided that some Van der Waals and frictional forces developed at the interface during deformations. Based on the experimental results the surface behavior is considered to be significant at higher shear rates.

The stepwise model development considering the concept of interface-induced stress-field is schematically represented in figure 8, prior to mathematical formulation. The stress-field, as shown at far right of this figure, was assumed to develop an exponentially decaying new modulus towards the matrix, analogous with the concept of boundary layer decay in a fluid flow through pipe. This part of modulus was taken as maximum at the platelet surface (y_{max}) and decayed to be minimum (zero) at the center of the matrix (y=0). The matrix is considered to exist between two consecutive and ideally parallel platelet surfaces.

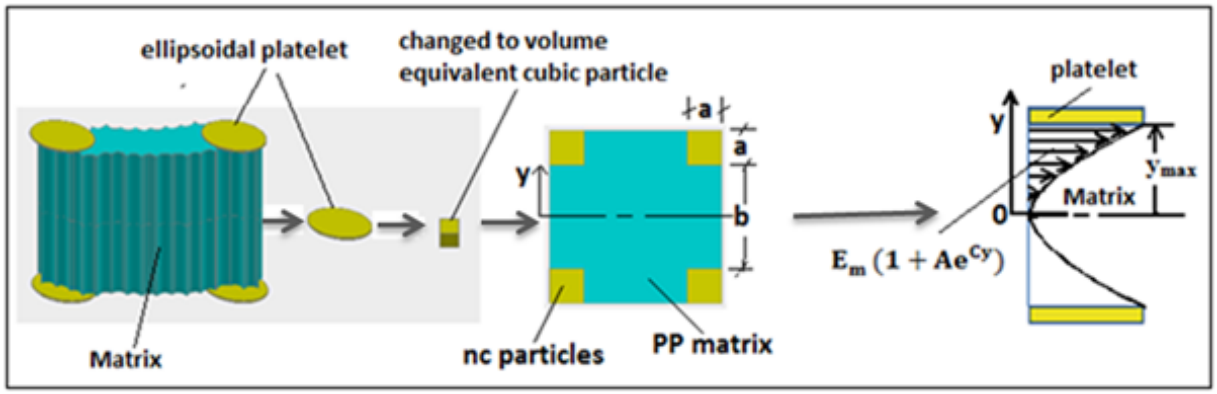

Figure 8. Stepwise model development of modulus on the interface-induced stress-field.

The assumptions in due consideration of this model are; (1) the perfectly exfoliated dispersion of nanoclay platelets distributed in a square lattice (as shown, second from right, in figure 8) throughout the PP matrix, (2) all platelets, actually, have ellipsoidal geometry and (3) consecutive platelet surfaces are parallel to each other. To support these assumptions in the formulation, the ellipsoidal geometry of platelets was changed to volume-equivalent cubic particles. The actual dimensions of the ellipsoidal platelets, as measured and reported by Cauvin (Cauvin et al., 2010), and parameter 'a' of the volume-equivalent cubic particle are given in figure 9 a & b, respectively. It should be noted that the same nanoclay platelets are used.

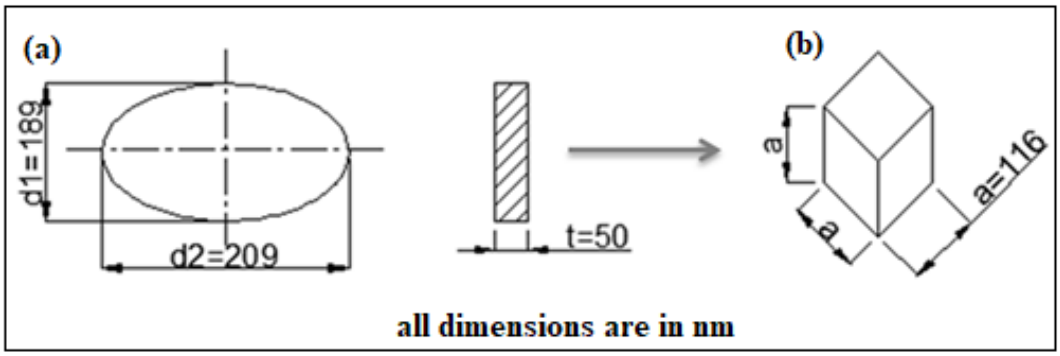

Figure 9. Dimensions of single nanoclay particle, (a) actual ellipsoidal platelet, and (b) volume equivalent cubic particle.

Modulus of the interface-induced stress-field represented as 'E_{sf}' was assumed to be an exponential function of matrix modulus 'E_m' and the surface-to-surface distance of two consecutive platelets 'y', as shown in equation (1).

$$E_{sf}(y) = E_m e^{Cy} \quad \text{.....1}$$

Where, 'y' is the location at which particular E_{sf} value is calculated and 'C' is a constant dependent on the respective elastic moduli of both the platelet 'E_p' and the matrix 'E_m' and surface-to-surface distance of two consecutive platelets. Boundary conditions (B.C.) given in equation (2) were applied by looking at the distribution of the stress-field, shown at far right portion of figure 8.

$$E_{sf}(y) = \begin{cases} E_m, @\ y = 0;\ B.c.1 \\ E_p, @\ y = y_{max};\ B.C.2 \end{cases} \quad \text{.....2}$$

Taking the first derivative of equation (1) with respect to 'y', making use of the given B.C.s and applying Euler's numerical approximations, the value of stress-field constant 'C' can be written as given in equation (3).

$$C = \frac{\ln\left(E_p/E_m\right)}{y_{max}} \quad \ldots\ldots 3$$

As this study focuses on the effect of nanoclay particles on mechanical properties of PP, it is considered that the interface-induced modulus is, fundamentally, due to the platelet surface. Hence, particle volume fraction V_p is made responsible to incorporate the E_{sf} in to the generally accepted rule of mixture to model modulus of the nano-reinforced composite 'E_c'. The new quasi-static model in the form of modulus factor (E_c/E_m) is, finally, given in equation (4).

$$E_c/E_m = 1 + V_p\left(E_p/E_m + Ae^{Cy}\right) \quad \ldots\ldots 4$$

Where, 'A' represents the following:

$$A = 1/2 \ln\left(\frac{E_p}{E_m}\right) \quad \ldots\ldots 5$$

To make use of the new model given in equation (4) one should fix V_p whereas elastic moduli E_p and E_m are given as 4.657 GPa and 0.83 GPa, respectively. Variables 'y' and 'y_{max}' should also be fixed and the stress field constant 'C' should subsequently be calculated. The variables are dependent on particle volume fraction V_p, the parameter 'a' of an ideal cubic particle and distance between surfaces of two consecutive particles shown by parameter 'b'. The variables and parameters are schematically depicted in figure 8 (second from right). To facilitate this, parameter 'a' of an ideal cubic particle was calculated by equating volume of the ellipsoidal platelet with volume of cubic particle as shown in equation (6).

$$\begin{cases} \text{Volume of Ellipsoidal platelet} = \text{Volume of Cubic particle} \\ \pi r_1 r_2 t = a^3 \\ r_1 \text{is major radius}, r_2 \text{is minor radius and t is thickness of the ellipsoid} \end{cases} \quad \ldots\ldots 6$$

As a result, parameter 'a' was calculated to be 116 nm, also shown in Figure 9 (b). However, y_{max} was calculated by putting 'a' as a function of 'b' and V_p.

$$a = V_p(a + b) \quad \ldots\ldots 7$$

Substituting 'b' by '$2y_{max}$', y_{max} can be written as;

$$y_{max} = 1/2\left(a/V_p - a\right) \quad \ldots\ldots 8$$

The primary model given in equation (4) was, in fact, developed based on quasi-static loading state. The quasi-static models considered in this study, together with the current model, are summarized as follows.

Current model: (equation (4))

Rule of mixture (Upper bound or Iso-strain model)

$$E_c = V_p E_p + V_m E_m \quad \text{.....9}$$

Halpin-Tsai model (Jones, 1999)

$$E_c/E_m = 1 + \xi\eta V_p \Big/ 1 - \eta V_p \quad \text{.....10}$$

Where,

$$\eta = \frac{E_p}{E_m} - 1 \Big/ \frac{E_p}{E_m} + \xi \quad \text{.....11}$$

While ξ is a measure of particle reinforcement that depends on particle geometry as given in equation (12).

$$\xi = 2\, b/t \quad \text{.....12}$$

Where, 'b' and 't' are breadth and thickness, respectively, of a particle with rectangular cross section. In this particular case, ellipsoidal platelets are considered. Thus, 'b' corresponds to the minor diameter 'd_1' and 't' corresponds to the thickness of the platelet, as shown in figure 9.

Takayanagi model (Takayanagi, Uemura and Minami, 1964; Okamoto and Takayanagi, 1968; Boumbimba et al., 2012).

$$E_c/E_m = \left[(1-\beta) + \left(\beta \Big/ 1 - \beta + \beta\left(\frac{E_p}{E_m}\right)\right)\right]^{-1} \quad \text{.....13}$$

Where, $\beta = \sqrt{V_p}$

Additional term which is a stand for dynamic loading condition is, then, incorporated in to the current model and the other existing quasi-static models. Finally, results of composite failure modulus factor at impact loading $\left(E_{fc}/E_{fm}\right)$, a ratio of failure modulus of the nano-composite 'E_{fc}' to that of matrix 'E_{fm}' at impact, based on the previous models were compared with the current model. The term modulus factor is used to be consistent with models of other past works. However, the new naming (failure modulus) referred with subscript 'f' stands for a limiting modulus regime observed prior to reaching of peak stress and is not associated with elasticity and yielding at such very high rates of loading. In other words, the elastic modulus regime of thermoplastics in quasi-static loading cases totally get transformed to visco-plastic stiffening regime in very-high strain

rate impacts, hence the term failure modulus. The comparison of failure modulus factors at varied particle volume fractions is shown in figure 10.

A new factor termed as DIFM (dynamic increase factor for modulus) was introduced and incorporated in to the quasi-static models to formulate a model for modulus at impact. The DIFM term particularly refers to the change in modulus from the small value of elastic nature at quasi-static loading to the raised (limiting or failure) value at impact loading. Therefore, failure modulus at impact loadings of the nano-composite (E_{fc}) given in equation (14) is found to be empirically dependent on DIFM of neat matrix denoted as D_m and particle weight fraction (W_p), in addition to the parameters considered in quasi-static models. The usage of W_p become appropriate after doing some trial-and-errors.

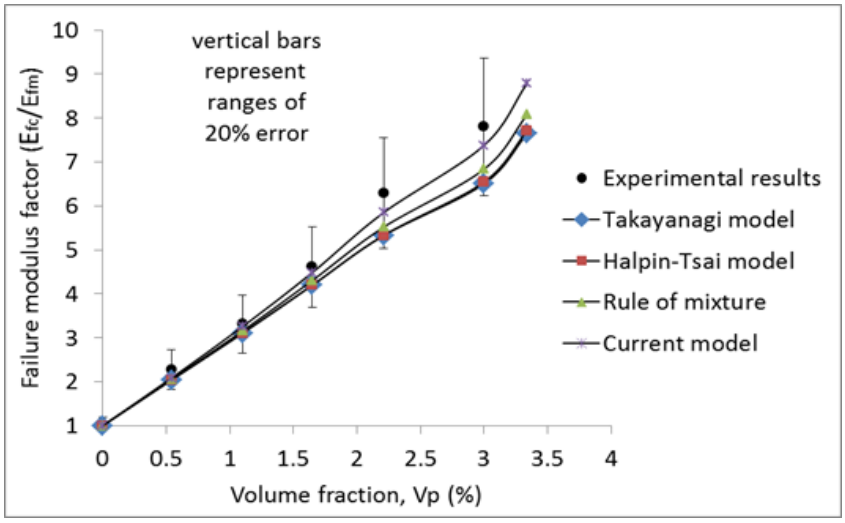

Figure 10. Failure modulus factor Vs particle volume fraction of PP nano-composites.

$$E_{fc} = D_m\left(1 + 100 * W_p\right)\left(E_{qc}\right) \quad \text{.....14}$$

Equations for E_{qc} (modulus of the composite at quasi-static loading) of all the models considered are the ones summarized above, which are simply written as E_c in equations (4, 9, 10 and 13). While, D_m is calculated as:

$$D_m = {E_{fm}}/{E_{qm}} \quad \text{.....15}$$

Where, E_{fm} is failure modulus of neat matrix at impact loading and E_{qm} is elastic modulus of neat matrix at quasi-static loading. Values of E_{qm} and E_{fm} were determined experimentally to be 0.83

GPa and 3.81 GPa, respectively. Hence, the value of D_m comes out to be 4.6 and substituted to equation (14).

As shown in figure 10, the new model is found to be the best representative of failure modulus for the nano-reinforced PP at high strain rate impacts. This can be understood from the error bars, showing 20% ranges of errors, at all experimental points. The new model depicts the preeminent agreement with the trend of experimental results having least average error (5 %) of all models. Rule of mixture become next to current model with 9 % average error, while Halpin-Tsai and Takayanagi models overlapped each other having same average error of 11.4 %. The model at impact loading is generally based on strain rate level to the order of 10^4 s^{-1}. Thus, one may consider some adjustments and experimental validations to use this model for lower and ultrahigh strain rate levels.

3.3.2. Peak Strength

Johnson-Cook (Johnson and Cook, 1985) and Omar et al. (Omar, Akil and Ahmad, 2011) models are considered and peak stress values of neat PP and the PP-nanocomposites are evaluated. Johnson-Cook model originally consists of strain hardening constants and temperature terms of flow stress which are ignored in this case. Thermoplastics do not have noticeable strain hardening region and the experiments in this study are conducted at average room temperature of 21±3^{o}C. Therefore, the simplified form of Johnson-Cook strength model given in equation (16) is adopted. Omar's strain rate sensitivity model used for neat polymers which is defined as equation (17) is completely adopted. When adopting these models the subscripts of nomenclatures are changed to the convenience of this study.

$$\sigma_{ip}/\sigma_{qp} = 1 + C * \ln\left(\dot{\varepsilon}_i/\dot{\varepsilon}_q\right) \quad \ldots\ldots 16$$

$$\sigma_{ip}/\sigma_{qp} = 1 + \beta/\sigma_{qp} * \ln\left(\dot{\varepsilon}_i/\dot{\varepsilon}_q\right) \quad \ldots\ldots 17$$

Where, σ_{ip} is peak stress at higher strain rate impact loading, σ_{qp} is peak stress at quasi-static loadings, $\dot{\varepsilon}_i$ is strain rate at impact loading and $\dot{\varepsilon}_q$ is strain rate at quasi-static loading. 'C' and 'β' are the dimensionless Johnson-Cook material constant and Omar's strain rate sensitivity in MPa, respectively. In the original Johnson-Cook model $\dot{\varepsilon}_q$ is represented as reference strain rate $\dot{\varepsilon}_o$ with a value of 1 s^{-1} assigned for convenience. However, the actual experimentally set $\dot{\varepsilon}_q$ value, 10^{-2} s^{-1}, is used here in this particular study.

Originally, equation (16) was formulated for strain rates of order of 10^3 s^{-1} and above and equation (17) was used for any strain rate up to 10^3 s^{-1} and no restriction was reported not to apply for higher strain rates. Considering the experimental results at quasi-static loading and that of averaged impact results, estimated values of 'C' and 'β' for all material systems are given in table 3.

Table 3. Estimated values of constants, C and β.

Constants	***Neat PP***	***PP+ 1wt%NC***	***PP+ 2wt%NC***	***PP+ 3wt%NC***	***PP+ 4wt%NC***	***PP+ 5wt%NC***
	Particle volume fractions, V_p (%)					
	0	0.54	1.10	1.65	2.21	3
C	0.55	0.57	0.59	0.65	0.70	0.75
β (MPa)	14.62	15.23	15.97	17.65	19.12	20.47

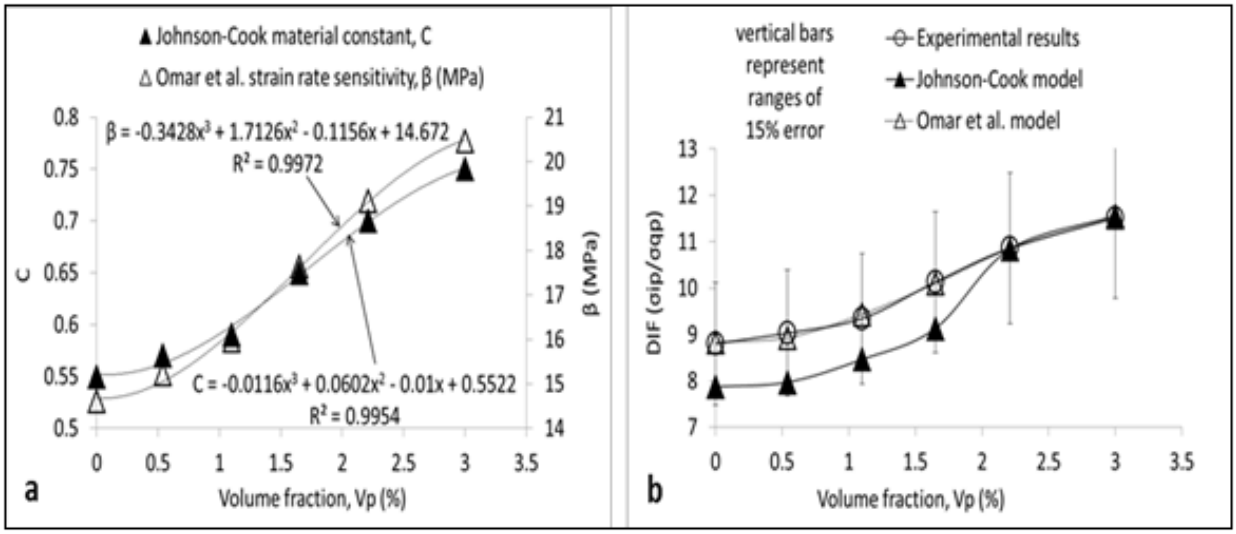

Figure 11. Strength models (a) cubic polynomial fitting of material constants (b) comparison of models and experimental result.

Noting the values of 'C' and 'β' in table 3, cubic polynomial curve fitting is found appropriate for both. Respective equations as functions of particle volume fraction (V_p) are generated in the plot itself and shown in figure 11a. Subsequently, stress factors, σ_{ip}/σ_{qp}, are calculated using both models for all V_p's and compared with experimental results (Fig 11b). Such a stress factor is termed as DIF (dynamic increase factor of flow stress) which is the ratio of peak stress at impact

to the peak stress at quasi-static loading. The term DIF was introduced by Lu and Li (2010) to observe the rate dependence of the flow stress of polymers.

Comparing the DIF's for each material system with corresponding estimations using the two models, Omar's model shows an interesting agreement with the experimental results (Fig 11b). Calculating the average errors, Johnson-Cook model incurs 7% while Omar's model experience negligible error (~0.5%). Thus, Omar's model seems applicable to predict impact strength values of material systems having closer strain rate dependence behaviors to PP and nano-composites.

4. CONCLUSION AND RECOMMENDATION

- At quasi-static loadings PP+5wt%NC is found to be the best performing material system in terms of all considered mechanical properties and the failure modes.
- Similar to the case in quasi-static loading, PP+5wt%NC show highest performance at high strain rate impacts due to the new dispersed induced deformation mechanics. When quantified in average-wise, improvements of 34 % in peak stress, 680 % in failure modulus and 80 % in toughness of PP+5wt%NC over neat PP are observed.
- Novel analytical model of failure modulus at impact is formulated for the nanoclay reinforced PP composite material systems. This new model is compared with Takayanagi model, Halpin-Tsai model and Rule of mixture and found to be the best representative of the experimental results.
- Simplified Johnson-Cook strength model and Omar's strain rate sensitivity model are applied to evaluate the peak stresses at high strain rate impacts of PP and PP nano-composites. Omar's model shows a toning agreement with the experimental results.
- Apart from being matrix for FRP composite body armor, such a performance of PP+5wt%NC and other comparable nano-reinforced matrices can foresee wider engineering applications. Areas where catastrophic failures are primary issues and high strength-to-weight ratio is the main design requirement: like in vehicle body structure, vibration damping and noise suppressions, damage protective panels, etc can be mentioned.

5. ACKNOWLEDGEMENTS

Authors are indebted to IRD-IITD for a grand challenge grant [MI00810] for doing the research project. First author is grateful to MOE-Government of Ethiopia for the scholarship.

6. REFERENCE

Boumbimba, R. M., Wang, K., Bahlouli, N., Ahzi, S., Rémond, Y & Addiego, F. 2012. Experimental investigation and micromechanical modeling of high strain rate compressive yield stress of a melt mixing polypropylene organoclay nanocomposites', *Mechanics of Materials*. Elsevier Ltd, **52**:58–68 (doi: 10.1016/j.mechmat.2012.04.006).

Cauvin, L., Kondo, D., Brieu, M & Bhatnagar, N. 2010. Mechanical properties of polypropylene layered silicate nanocomposites: Characterization and micro-macro modelling. *Polymer Testing,* **29(2)**:245–250 (doi: 10.1016/j.polymertesting.2009.11.007).

Gebremeskel, S. A., Asija, N., Priyanshu, A., Chouhan, H & Bhatnagar, N. 2014. Design customization and development of Split Hopkinson Pressure Bar for light and soft armour materials. *Global Journal of Researches in Engineering A: Mechanical and Mechanics Engineering*, **14(7)**:62–75.

Gebremeskel, S. A., Asija, N., Chouhan, H & Bhatnagar, N. 2017. Appraisal of strain rate sensitivity of polypropylene nanocomposites. *Procedia Engineering*, **173**:800-806 (doi: 10.1016/j.proeng.2016.12.103).

Gebremeskel, S. A & Bhatnagar, N. 2015. Effect of high impact loading on nanoclay reinforced polypropylene. *Journal of Materials Science and Engineering*, **4(6)**:207 (doi: 10.4172/2169-0022.1000).

Grujicic, M., Pandurangan, B., Zecevic, U., Koudela, K. L & Cheeseman, B. A. 2007. Ballistic performance of Alumina/S-2 glass-reinforced polymer-matrix composite hybrid lightweight armor against armor piercing (AP) and non-AP projectiles. *Multidiscipline Modeling in Materials and Structures*, **3(3)**:287–312.

Hedayati, A & Arefazar, A. 2009. Multi-scale analysis of polypropylene based organoclay containing composites, Part 1: Morphology. *Polymer Testing,* **28(2)**:128–138 (doi: 10.1016/j.polymertesting.2008.10.007).

Ji, X. L., Jing, J. K., Jiang, W & Jiang, B. Z. 2002. Tensile modulus of polymer nanocomposites. *Polymer Engineering & Science*, **42(5)**:983–993.

Johnson, G. R & Cook, W. H. 1985. Fracture characteristics of three metals subjected to various strains, strain rates, temperatures and pressures. *Engineering Fracture Mechanics*, **21(1)**: 31-48.

Jones, R. M. 1999. *Mechanics of composite materials*. 2nd edition, ISBN: 1-56032-712-X, Taylor

& Francis,519p.

Kukureka, S. N & Hutchings, I. M. 1981. Measurement of the mechanical properties of polymers at high strain-rates by Taylor impact. 7th International Conference on High Energy Rate Fabrication, University of Leeds, pp29-38.

Li, Z & Lambros, J. 2001. Strain rate effects on the thermomechanical behavior of polymers. *International Journal of Solids and Structures*, **38(20)**:3549–3562.

Lu, Y. B & Li, Q. M. 2010. Dynamic behavior of polymers at high strain-rates based on Split Hopkinson Pressure Bar tests. *International Journal of Impact Engineering*, **38(1)**:41-50 (doi: 10.1016/j.ijimpeng.2010.08.001).

Odegard, G. M., Clancy, T. C & Gates, T. S. 2005. Modeling of the mechanical properties of nanoparticle/polymer composites. *Polymer*, **46(2)**:553-562 (doi:10.1016/j.polymer.2004. .11.022).

Okamoto, T & Takayanagi, M. 1968. Application of two-phase mechanical model to visco- elastic properties of blends of high-density and low-density polyethylene. *Journal of Polymer Science Part C: Polymer Symposia*, **23(2)**:597–606.

Omar, M. F., Akil, H. M & Ahmad, Z. A. 2011. Measurement and prediction of compressive properties of polymers at high strain rate loading. *Materials & Design*, **32(8-9)**:4207–4215 (doi: 10.1016/j.matdes.2011.04.037).

Park, M., Yoo, J & Chung, D. T. 2005. An optimization of a multi-layered plate under ballistic impact. *International Journal of Solids and Structures*, **42(1)**:123–137 (doi: 10.1016/j.ijsolstr.2004.07.008).

Qiao, P., Yang, M & Bobaru, F. 2008. Impact mechanics and high-energy absorbing materials: Review. *Journal of Aerospace Engineering*, **21(4)**:235–248 (doi: 10.1061/(ASCE)0893-1321(2008)21).

Rajendran, A. M. 1994. Modeling the impact behavior of AD85 ceramic under multiaxial loading. *International Journal of Impact Engineering*, **15(6)**:749–768.

Shariatpanahi, H., Sarabi, F., Mirali, M., Hemmati, M & Mahdavi, F. 2009. Polypropylene-organoclay nanocomposite : Preparation , microstructure , and mechanical properties. *Journal of Applied Polymer Science*, **113(2)**:922–926.

Silva, M. A. G., Cismasiu, C & Chiorean, C. G. 2003. Low velocity impact on laminates reinforced with polyethylene and aramidic fibres. 9th International Conference on Enhancement and

Promotion of Computational Methods in Engineering and Science, London, Taylor & Francis, pp843–851.

Silva, M. A. G., Cismasiu, C & Chiorean, C. G. 2005. Numerical simulation of ballistic impact on composite laminates. *International Journal of Impact Engineering*, **31(3)**:289-306 (doi: 10.1016/j.ijimpeng.2004.01.011).

Takayanagi, M., Uemura, S & Minami, S. 1964. Application of equivalent model method to dynamic rheo-optical properties of crystalline polymer. *Journal of Polymer Science Part C: Polymer Symposia*, **5(1)**:113–122.

Valavala, P. K & Odegard, G. M. 2005. Modeling techniques for determination of mechanical properties of polymer nanocomposites. *Rev. Adv. Mater. Sci*, **9**:34–44.

Vedantam, K. Bajaj, D., Brar, N. S & Hill, S. 2006. Johnson-Cook strength models for mild and DP 590 steels. In: M.D.Furnish et al. (eds) *Shock Compression of Condensed Matter*. American Institute of Physics, pp775–778.

Yong, M., Iannucci, L & Falzon, B. G. 2010. Efficient modelling and optimisation of hybrid multilayered plates subject to ballistic impact. *International Journal of Impact Engineering*, **37(6)**:605–624 (doi: 10.1016/j.ijimpeng.2009.07.004).

Yuan, Q & Misra, R. D. K. 2006. Impact fracture behavior of clay–reinforced polypropylene nanocomposites. *Polymer*, **47(12)**:4421–4433 (doi: 10.1016/j.polymer.2006.03.105).

Zhu, L & Narh, K. A. 2004. Numerical simulation of the tensile modulus of nanoclay-filled polymer composites. *J. Polymer Science Part B: Polymer Physics*, **42(12)**:2391–2406 (doi: 10.1002/polb.20112).